Turbulent boundary layer measurements over permeable surfaces

Christoph Efstathiou

Dept. of Aerospace and Mechanical Engineering
University of Southern California
Los Angeles, California 90089
efstathi@usc.edu

Mitul Luhar

Dept. of Aerospace and Mechanical Engineering
University of Southern California
Los Angeles, California 90089
luhar@usc.edu

ABSTRACT

Laser Doppler Velocimetry (LDV) measurements were made in turbulent boundary layers over a flat plate. Commercially available, open cell foams with pore sizes varying from 0.3-2mm were flush mounted into a cutout in the downstream half of the plate. The friction Reynolds number over the smooth wall upstream of the porous section was $Re_\tau \approx 1690$. Measurements made to within 140μm (3-4 viscous units) of the porous interface revealed a substantial slip velocity at the interface ($> 30\%$ of the free stream velocity) that was approximately constant across changing substrate geometry. A mean velocity deficit, increasing with pore size, was observed further from the wall in the region corresponding to the log-layer in smooth wall boundary layers. For all foams, an elevated streamwise turbulence intensity was found further into the boundary layer (until $y/\delta \approx 0.2$). An outer peak in turbulence intensity was found for the largest pore sizes.

INTRODUCTION

Turbulent flows of scientific and engineering interest are often bounded by walls that are not smooth, solid, or uniform. Manufacturing techniques, operational requirements and natural evolution often lead to non-uniform, rough or porous boundaries, for example in flows over heat exchangers, forest canopies, bird feathers and rivers. Such substrates can be characterized by porosity, ε, permeability, k, and drag length scale, $(C_d a)^{-1}$, where C_d is the drag coefficient, and a is the frontal area per unit volume (Ghisalberti, 2009). Porous boundaries also enable active flow control through suction and blowing. Despite these applications, relatively little is known about the relationship between turbulent flows and porous substrates. As a result, there are few models that can *predict* how a porous substrate of known geometry will influence a mean flow field and turbulent velocity spectra.

Previous direct numerical simulations (DNS) over porous surfaces (Breugem *et al.* (2006); Chandesris *et al.* (2013); Jimenez *et al.* (2001)) have found some support for a shifted logarithmic region in the mean velocity profile and a varying von Kármán constant (κ). These simulations have also identified a Kelvin-Helmholtz type instability as a characteristic flow feature. However, such simulations are limited to low Reynolds numbers of $Re_\tau = \mathcal{O}(10^2)$, and rely on simplified models for the porous medium. Breugem *et al.* (2006) solve the volume-averaged Navier-Stokes equations inside the porous medium and at the interface. For closure, this requires additional information about the stresses inside the porous medium depending on the pore geometry and Reynolds number. Another approach, employed by Jimenez *et al.* (2001), is to impose vertical velocity fluctuations proportional to pressure fluctuations at the porous boundary of the form $v = -\beta p$.

Previous experiments by Zagni & Smith (1976), Kong & Schetz (1982) and Manes *et al.* (2011) have examined the effect of a range of substrate geometries including perforated surfaces, packed spheres and foam mattresses at Reynolds numbers $Re_\tau = \mathcal{O}(10^3)$. These experiments have generated results that are broadly consistent with the simulations, but they include limited near-wall measurements. The experiments described below begin to address some of these limitations.

EXPERIMENTAL METHODS

The experiments were conducted in the USC water channel, a free-surface, recirculating facility with test section dimensions of 762 cm length, 89 cm width and 48 cm water depth. At a free-stream velocity of 60 cm/s, the background turbulence intensity is $\leq 1\%$. The temperature for all experiments was $23 \pm 0.5^\circ$ for which the kinematic viscosity is $\nu = 0.93 \times 10^{-2}$ cm^2/s. A 240 cm long flat plate was suspended from precision rails at a height $H = 30$ cm above the test section bottom. To avoid free-surface effects, measurements were made below the flat plate. The confinement between the flat plate and bottom of the channel naturally led to a slightly favorable pressure gradient and slight free stream velocity increase along the plate ($\leq 3\%$), however the non-dimensional acceleration parameter, $\Lambda = \frac{\nu}{U_e^2}\frac{dU}{dx}$ was on the order of 10^{-8} suggesting any pressure gradient effects are likely to be mild.

The flow was tripped by a wire of 0.5mm diameter 5cm downstream of the leading edge. A cutout of length 89cm and width 60cm was located 130cm downstream of the leading edge. Smooth and porous surfaces were substituted into the cutout, flush with the smooth plate around it. The porous test specimens, described in further detail below, were bonded to a solid Garolite^{TM} sheet to provide a rigid structure and prevent bleed through. The thickness of the porous substrates was $h = 12.7$mm. See Fig, 1 for more detail.

Streamwise velocity measurements were made at the channel centerline using a Laser Doppler Velocimeter (LDV, MSE Inc.) with a 50cm standoff distance and measurement volume of 300μm by 150μm by 1000μm (x by y by z). The large standoff distance required to measure at the channel centerline reduced data rates to 50Hz in the freestream and $<$ 1Hz at the stations closest to the wall. A minimum of 800 data points in the regions with the lowest velocity and 4000-25000 data points in regions of higher velocity were collected to ensure fully converged statistics. Inverse velocity weighting, as described by McLaughlin & Tiederman (1973), was used to offset the increased number of higher velocity particles moving through the measurement volume in a flow of uniform seeding. The LDV was mounted on a precision traverse with 16μm resolution. Near the wall, measurements were made at stations 30μm (20% of the measurement volume dimension in y) apart. In all cases, the location of the wall was taken to be the station where no more particles passed through the measurement volume. The uncertainty in the wall location was estimated to be less than the dimension of the measurement volume in the vertical

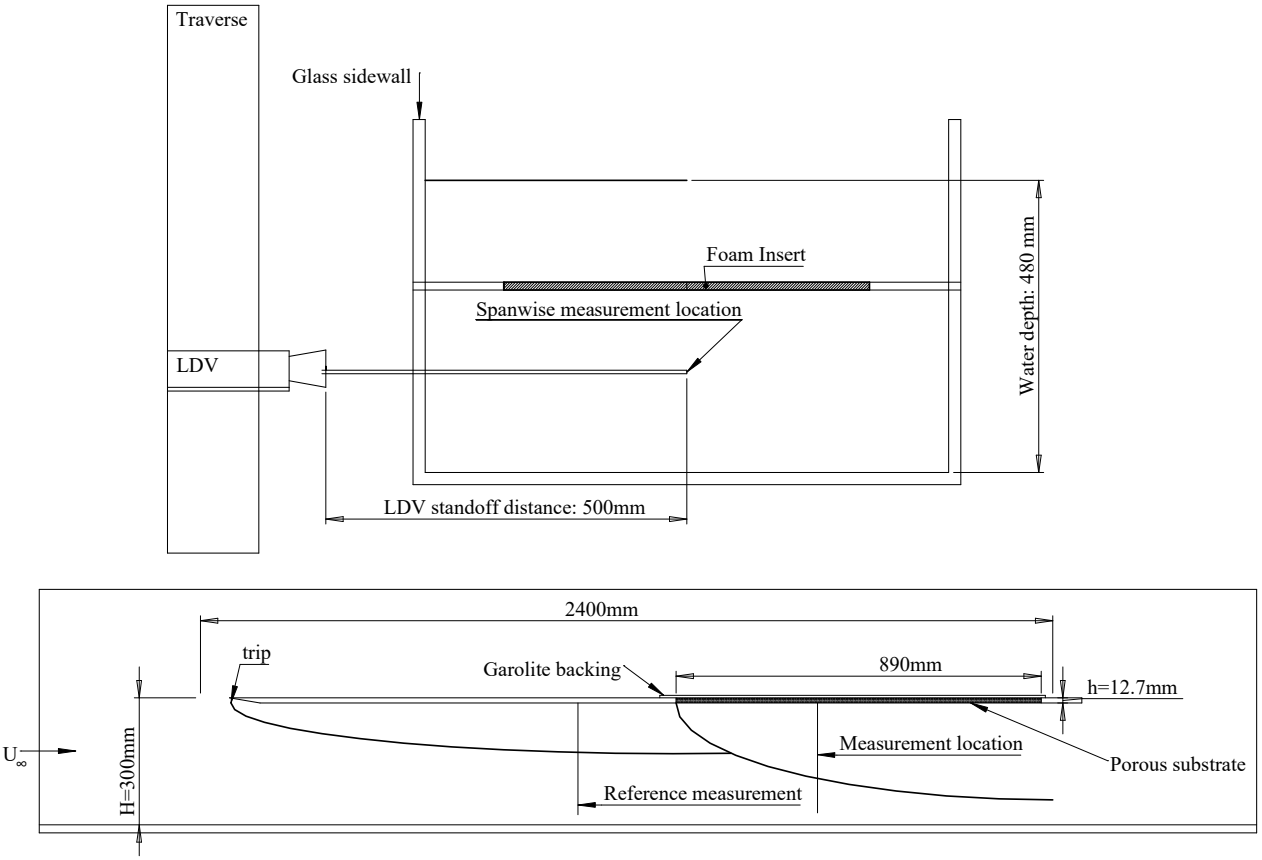

Figure 1. Experimental illustration showing wall normal-spanwise (top) and streamwise-wall normal (bottom) views. Measurements were made upstream of the porous substrate for reference and at one location $x/h = 42$, where $x = 0$ is defined as the smooth-porous transition point.

direction, $y_0 < 150\mu$m. The measurement uncertainty was $\leq 1\%$ in the mean velocity and velocity fluctuations, with the maximum near the interface. For the smooth wall profile, the friction velocity, u_τ was estimated in two ways. First, inside the viscous sublayer the velocity profile was assumed to be of form $U^+ = y^+$. Utilizing a linear curve fit over the first 5-9 points, the friction velocity was estimated to be $u_\tau = 22.6$mm/s. Secondly, a linear fit in the log-layer using constants $\kappa = 0.38$, $B = 5$ yielded $u_\tau = 23$mm/s. With these estimates of friction velocity, the friction length scale is $\nu/u_\tau = 40\mu$m.

Four commercially available, open cell, reticulated foams were used as permeable substrates. The nominal pore count was 10-100ppi (pores per inch). Photographs of thin sections of the foams are provided in Fig. 2. The pore size distribution for each foam was estimated via image analysis. The mean pore-size range was $s = 2.1 \pm 0.3$mm for the 10ppi foam to $s = 0.29 \pm 0.02$mm for the 100ppi foam. The permeabilities, estimated from pressure drop charts available online, range from $k = 110 \times 10^{-9}$ m^2 for the 10 ppi foam to $k = 6 \times 10^{-9}$ m^2 for the 100 ppi foam. Foam properties are provided in Table 1. Per the manufacturer, the porosity of each foam was 97%. This was confirmed to within 0.5% via measurements that involved submerging the foams in water to measure solid volume displacements.

Foam	k (10^{-9}m^2)	s (mm)	Re_k	s^+	h/s
10 ppi	110	2.1 ± 0.3	8.2	52	6.0
20 ppi	60	1.5 ± 0.2	6.1	37	8.5
60 ppi	10	0.40 ± 0.03	2.5	10	32
100 ppi	6	0.29 ± 0.02	1.9	7	44

Table 1. Permeability (k), average pore sizes (s), and related dimensionless parameters for tested foams. Note that $s^+ = su_\tau/\nu$ and $Re_k = \sqrt{k}u_\tau/\nu$ are defined using the friction velocity upstream of the porous section.

RESULTS

Mean velocity profiles were collected at the centerline of the channel at a location 60% of the length of the cutout from the substrate transition point. This corresponds to $x/h = 42$, where h is the foam thickness. Independent measurements confirmed that the internal boundary layer originating at the transition in surface geometry is fully developed by $x/h \approx 40$ for all foams. The mean velocity profiles (U) normalized by the external velocity U_e and

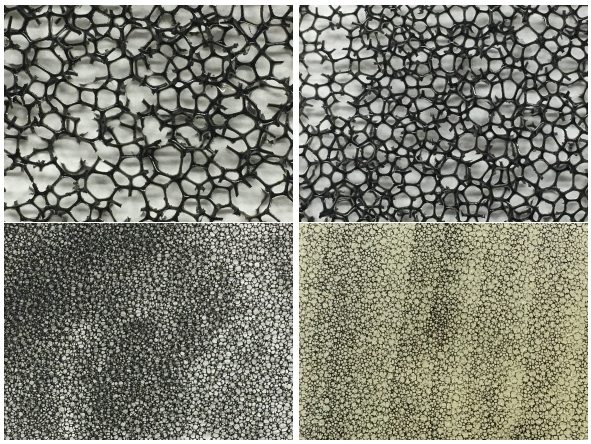

Figure 2. Photographs showing thin sheets of the 10, 20 (top) and 60,100 (bottom) ppi foams.

the local boundary layer thickness, δ_{99} are shown in Fig. 3, the streamwise fluctuation (u) profiles in Fig. 4 and the skewness profiles in Fig. 5.

The mean velocity profile is modified in two significant ways with respect to the smooth wall profile taken upstream. A substantial slip velocity was found near the porous substrate. This slip velocity was found to be approximately 30% of the external velocity across all substrates. The observed slip velocity is consistent with the VANS simulation by Breugem *et al.* (2006), who observed a slip velocity of approximately 30% only for their highest porosity case ($\varepsilon = 0.95$, $Re_k = 9.35$). Note that the substrate properties for the foams (listed in 1) are close to the properties of the simulation.

Secondly, a mean velocity deficit was found from $0.004 \leq y/\delta \leq 0.4$. The deficit increased with increasing pore size. A maximum deficit of 15% for the least permeable foam to almost 50% for the 20ppi foam relative to the smooth wall profile was measured. Non-monotonic behavior was observed with the velocity deficit for the largest pore sizes (10ppi, $s^+ = 52$) found to be smaller than the deficit over foam with pore sizes of $s^+ = 37$ (20ppi). In the wake region, the velocity profiles collapsed onto the canonical velocity profile again.

The mean streamwise turbulence intensities ($\overline{u^2}/U_e^2$) are shown in Fig. 4. Near the wall, the fluctuations are several times higher than in the viscous sublayer near smooth walls. No laminar sublayer exists near the porous interface. However, the near wall peak characteristic of smooth wall turbulent boundary layers is missing. The turbulence intensity is lower than the peak seen in the smooth wall upstream, and remains elevated further into the boundary layer. At $y/\delta \approx 0.01$, a significant difference between small pores ($Re_k \leq 5$) and large pores emerges. The boundary layer over the large pores is distinguished by a peak in $\overline{u^2}$ located near $y/\delta \approx 0.1$, while $\overline{u^2}$ remains approximately constant over the lower permeability substrates. We hypothesize that this outer peak is associated with structures resembling Kelvin-Helmholtz vortices. Experiments designed to test this hypothesis are ongoing. In the wake region ($y/\delta > 0.4$), the data collapse onto the smooth wall profile. Note that the observed reduction in streamwise turbulent intensity is consistent with the observations made by Breugem et al. (2006) and Manes et al. (2011).

The skewness of the measured velocities is shown in Fig. 5. In contrast to the smooth wall profile, over the foam substrates the sign of the skewness is positive until $y/\delta \approx 0.1$. Note that the change in sign of the skewness corresponds to the location of the outer peak in streamwise velocity observed over the foam substrates. Further, the magnitude of the skewness generally increases with pore size, which is consistent with the intensity measurements (the 10 and 20 ppi cases again show non-monotonic behavior). These observations are particularly interesting given the intrinsic link between skewness and the amplitude modulation phenomenon (see e.g. Marusic *et al.* (2010), Duvvuri & McKeon (2015)). The idea that the so-called very large scale motions (VLSMs) in the logarithmic region of the flow have a modulating effect on the intensity of the near-wall turbulence has led to the development of a promising class of predictive models for smooth wall turbulent flows. The energetic structures giving rise to the outer peak in streamwise intensity observed over the porous foams may have a similar modulating effect on the turbulence close to the porous interface.

Without a direct measurement of the wall shear stress or the wall normal velocities near the wall, an independent estimate of the friction velocity u_τ and log-law constants κ and B is not possible. An alternative non-dimensionalization in terms of U_e and δ, is needed. The mean velocity profile of a turbulent boundary layer over smooth and rough surfaces is described by

$$\frac{U}{u_\tau} = \frac{1}{\kappa}\log(y^+ + y_s^+) + B + w(y/\delta)\frac{\Pi}{\kappa} - \Delta U^+ \qquad (1)$$

The rough wall formulation may hold for boundary layers over porous media, provided y is shifted up by an amount y_s^+. The logarithmic layer, multiplied by u_τ/U_e is described by

$$\frac{U}{U_e} = \frac{u_\tau}{U_e\kappa}\log\frac{y+y_s}{\delta} + D \qquad (2)$$

where y_s is a shift of the logarithmic layer origin towards the permeable substrate, and D accounts for the constant B as well as a change of wall normal units to y/δ. Taking the derivative with respect to y, $(y+y_s)\frac{\partial U}{\partial y} = \frac{u_\tau}{\kappa}$,where $\frac{u_\tau}{\kappa}$ is assumed to be constant. This allows the estimation of u_τ/κ and y_s, but not u_τ and κ independently. The wall normal gradient, $\frac{y}{U_e}\frac{\partial U}{\partial y}$ is shown in Fig. 6. Fitting over the range $0.02 < y/\delta < 0.2$, where the normalized gradient is taken as constant, $u_\tau/\kappa U_e$ can be estimated and is shown in Fig. 7. The red cross indicates the estimate for u_τ over the smooth wall obtained from a least squares fit in the near-wall region using an assumed κ. These fits suggest that the value of u_τ/κ increases with increasing pore size, though there is some evidence of saturation. This saturation is consistent with the non-monotonic behavior observed in the mean velocity and streamwise intensity profiles, whereby the 10ppi and 20ppi foams had a similar effect on the flow. Note that the estimates for u_τ/κ were very sensitive to the range of y/δ employed in the fitting procedure, though the overall trends remained similar. As such the exact values of u_τ/κ provided in Fig. 7 must be treated with caution.

CONCLUSIONS

The results presented above show that turbulent boundary layers over high-porosity surfaces are modified substantially compared to canonical smooth wall flows. Measurements made to within 4 viscous units of the porous interface found a near-constant slip velocity ($\approx 0.3U_e$) across the substrates tested. In the region where a logarithmic layer is found in canonical, smooth-wall boundary layers, a significant mean velocity deficit of up to

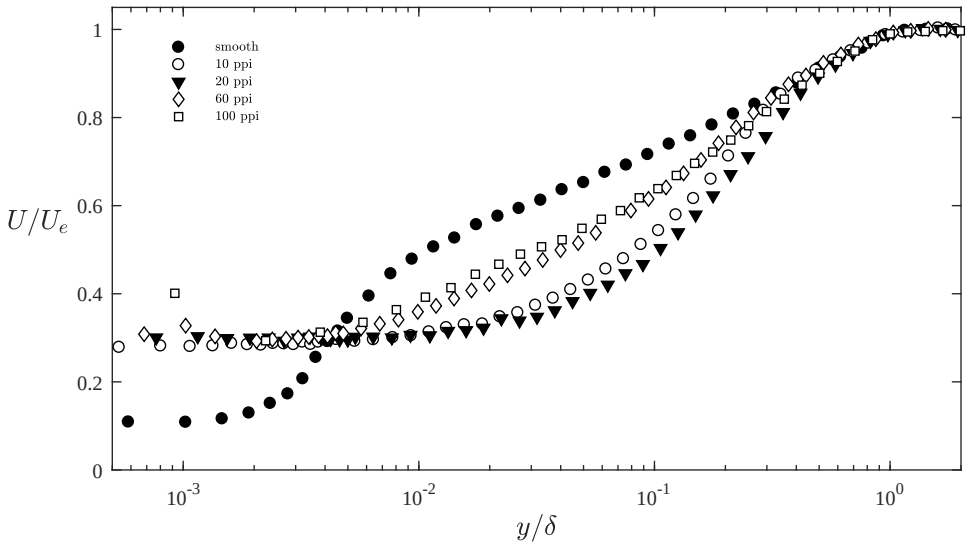

Figure 3. Mean velocity profiles over permeable substrates with normalized pore sizes of $s^+ = 7 - 52$.

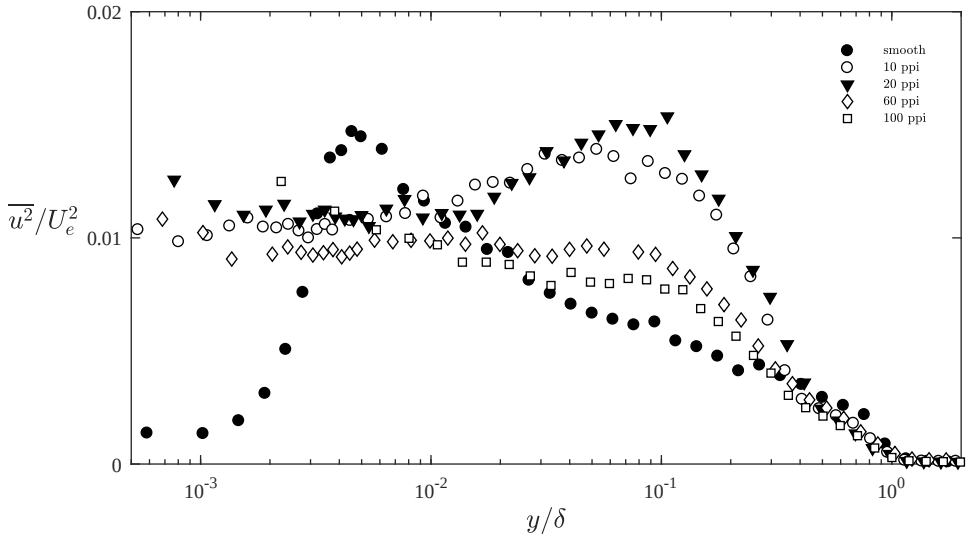

Figure 4. Mean streamwise turbulence intensity profiles over substrates with pore sizes ranging from $s^+ = 7 - 52$.

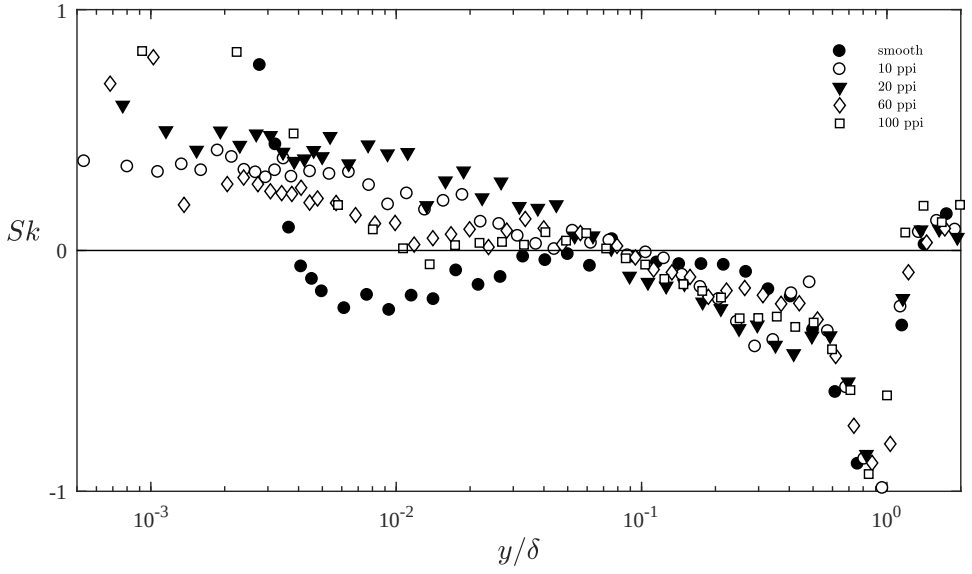

Figure 5. Mean streamwise velocity skewness profiles acquired over porous substrates with pore sizes ranging from $s^+ = 7 - 52$.

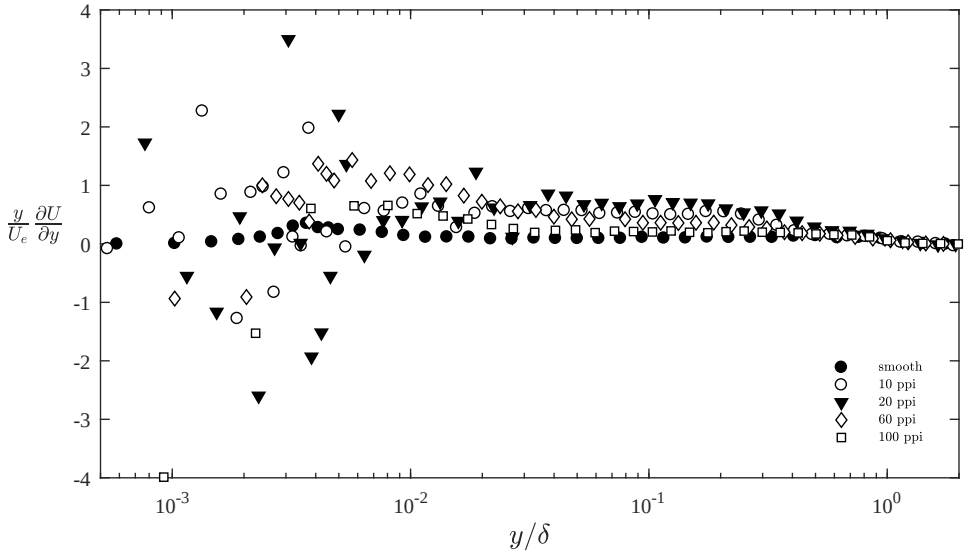

Figure 6. Mean streamwise velocity skewness profiles acquired over porous substrates with pore sizes ranging from $s^+ = 7 - 52$.

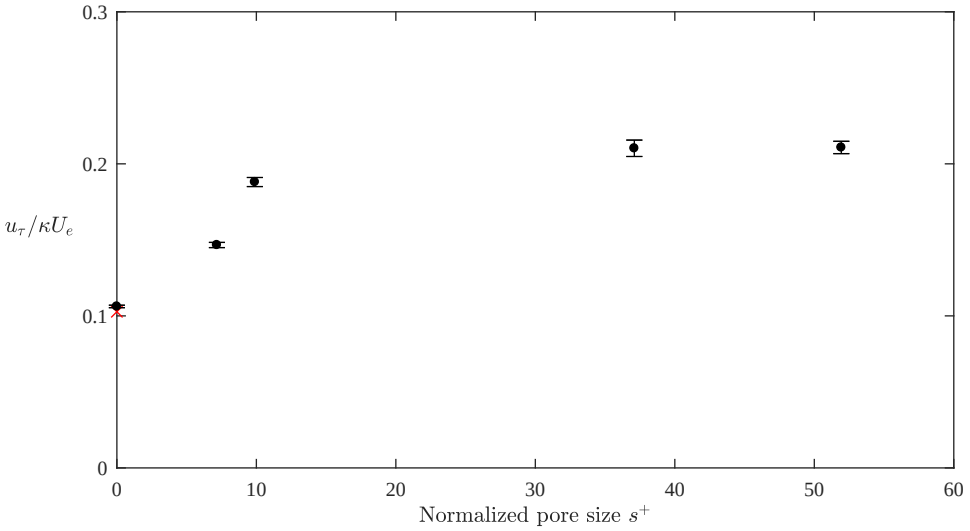

Figure 7. Log-law slope ($u_\tau/\kappa U_e$) obtained by fitting over the region of approximately constant velocity gradient. Uncertainty was estimated by varying the range of the curve fit. The red cross indicates the value obtained for u_τ for the smooth wall by assuming κ and fitting the friction velocity to the log-layer.

50% was observed. In this part of the boundary layer, elevated streamwise turbulence intensity was observed. The inner peak in $\overline{u^2}$ found in smooth wall boundary layers is replaced by a plateau of lower magnitude extending from the interface to $y/\delta \leq 0.2$ for smaller pore sizes, while an outer peak was found for the largest pore sizes. This outer peak may be attributed to Kelvin-Helmholtz type vortices. The skewness profiles suggest that these outer structures may also have an amplitude modulation type effect on the near-wall turbulence. A near-constant value of $y\frac{\partial U}{\partial y}$ in the region $0.05 \leq y/\delta \leq 0.2$ supports the existence of a shifted logarithmic region with modified slope.

Acknowledgments

This work was supported by the Air Force Office of Scientific Research under AFOSR grant No. FA9550-17-1-0142 (Program Manager: Dr. Douglas Smith).

REFERENCES

Breugem, WP, Boersma, BJ & Uittenbogaard, RE 2006 The influence of wall permeability on turbulent channel flow. *Journal of Fluid Mechanics* **562**, 35–72.

Chandesris, Marion, d'Hueppe, A, Mathieu, Benoit, Jamet, Didier & Goyeau, Benoit 2013 Direct numerical simulation of turbulent heat transfer in a fluid-porous domain. *Physics of Fluids* **25** (12), 125110.

Duvvuri, Subrahmanyam & McKeon, Beverley J 2015 Triadic scale interactions in a turbulent boundary layer. *Journal of Fluid Mechanics* **767**, R4.

Ghisalberti, Marco 2009 Obstructed shear flows: similarities across systems and scales. *Journal of Fluid Mechanics* **641**, 51–61.

Jimenez, Javier, Uhlmann, Markus, Pinelli, Alfredo & Kawahara, Genta 2001 Turbulent shear flow over active and passive porous surfaces. *Journal of Fluid Mechanics* **442**, 89–117.

Kong, F & Schetz, J 1982 Turbulent boundary layer over porous surfaces with different surfacegeometries. In *20th Aerospace Sciences Meeting*, p. 30.

Manes, Costantino, Poggi, Davide & Ridolfi, Luca 2011 Turbulent boundary layers over permeable walls: scaling and near-wall structure. *Journal of Fluid Mechanics* **687**, 141–170.

Marusic, I, Mathis, R & Hutchins, N 2010 Predictive model for wall-bounded turbulent flow. *Science* **329** (5988), 193–196.

McLaughlin, DK & Tiederman, WG 1973 Biasing correction for individual realization of laser anemometer measurements in turbulent flows. *The Physics of Fluids* **16** (12), 2082–2088.

Zagni, Anthony FE & Smith, Kenneth VH 1976 Channel flow over permeable beds of graded spheres. *Journal of the Hydraulics Division* **102** (2), 207–222.